

# Particle Dynamics in a Dielectrophoretic Microdevice

S.T. Wereley and I. Whitacre

Purdue University, School of Mechanical Engineering,  
West Lafayette, IN 47907-2088, USA, wereley@purdue.edu

## ABSTRACT

Micro particle image velocimetry ( $\mu$ PIV) has been effectively used to measure fluid velocities in micron scale devices, such as a microchannel with moderate depth. Measurements of pressure driven flows through very shallow or thin microchannels can be obscured by depthwise velocity gradients which deform cross-correlation peaks used to measure velocity. Two methods are proposed for deducing velocity distributions from cross-correlation-based PIV measurements. One method, the deconvolution method, involves deconvolving a cross-correlation with an autocorrelation. This method is shown to approximate velocity distributions, but was found to be sensitive to noise in correlations and is subject to spurious oscillations. A second method, the synthetic image method, was developed to improve upon the successes of the deconvolution method. This method involves extracting the locations of particles in a PIV recording and generating simulated particle images with a prescribed single pixel particle intensity distribution. This method was found to accurately predict simulated and experimental velocity distributions. These methods are benchmarked with simulated case studies, and used to measure velocity distributions in a dielectrophoretic particle trapping device. The dielectrophoretic forces are seen to cause the particle to migrate toward the top of the device and to trap them near the leading edge of each electrode.

## 1 INTRODUCTION AND SET UP

### 1.1 DEP Device

A dielectrophoretic device has been designed to trap, separate, and concentrate biological components carried in solution. The operating principle of the device is the dielectrophoretic interaction between the spheres and the fluid. The device was designed and manufactured by Haibo Li at Purdue University, a student in Prof. Bashir's research group (Li, et al, 2004). The device consists of a microchannel with a depth of 11.6  $\mu\text{m}$ , width of 350  $\mu\text{m}$ , and length of 3.3 mm. The channel was anisotropically etched in silicon to produce a trapezoidal cross-section. The channel was covered by a piece of anodically bonded glass. A schematic view and digital photo of the device are shown in Figure 1. Bright regions represent platinum electrodes and the dark regions represent the electrode gaps. The electrodes are covered by a 0.3  $\mu\text{m}$  thick layer of PECVD silicon dioxide, which insulates the electrodes from the liquid medium, suppressing electrolysis. The electrodes are arranged in interdigitated pairs so that the first and third electrodes from Figure 1 are always at the same potential. The second and fourth electrodes are also at the same potential, but can be at a different potential than the first and third electrodes. An alternating electric potential is applied to the interdigitated electrodes to create an electromagnetic field with steep spatial gradients. Particle motion through the resulting electric field gradients causes polarization of the suspended components, resulting in a body force that repels particle motion into increasing field gradients. In the experiments, sample solutions were injected into the chamber using a syringe pump (World Precision Instruments Inc., SP200i) and a 250 $\mu\text{l}$  gas-tight luer-lock syringe (ILS250TLL, World Precision Instruments Inc.). The flow rate could be adjusted and precautions were taken to avoid air bubbles. An HP 33120A arbitrary waveform generator was used as the AC signal source to produce sinusoidal signal with frequency specified at 1MHz.

### 1.2 Micro Particle Image Velocimetry

Images of the particles were acquired using a standard  $\mu$ PIV system. In these experiments a mercury lamp is used to illuminate the 0.7  $\mu\text{m}$  polystyrene latex (PSL) microspheres (Duke Scientific) that are suspended in de-ionized water in concentrations of about 0.1% by volume. The particles are coated with a red fluorescing dye ( $\lambda_{\text{abs}}=542\text{ nm}$ ,  $\lambda_{\text{emit}}=612\text{ nm}$ ). The images were acquired using a Photometrics CoolSNAP HQ interline transfer monochrome camera (Roper Scientific). This camera is capable of 65% quantum efficiency around the 610 nm wavelength. The largest available image size that can be accommodated by the CCD array is 1392 by 1040 pixels, but the camera has the capability of pixel binning, which can drastically increase the acquisition frame rate by reducing the number of pixels that need to be digitized. A three-by-three pixel binning scheme was used in this experiment, producing images measuring 464 by 346 pixels, which were captured at a speed of 20 frames per second. The average focused particle diameter in the images was approximately 3 pixels.

#### *Shallow Channel Considerations*

When performing  $\mu$ PIV measurements on shallow microchannels, the depth of focus of the microscope can be comparable in size to the depth of the flow. A PIV cross-correlation peak, the location of which is the basis for conventional PIV velocity measurements, is a combination of the velocity distribution in the interrogation region and some function of average particle

shape. PIV velocity measurements containing velocity gradients can substantially deviate from the ideal case of depthwise uniform flow. Gradients within the light sheet plane have been addressed by image correction techniques (Wereley, et al., 2002), but gradients in the depthwise direction remain problematic. They can cause inaccurate velocity measurements due to the presence of multiple velocities within an interrogation region that are independent of mesh refinement. One problem with depthwise velocity gradients is cross-correlation peak deformation which reduces the signal to noise ratio of a PIV measurement (Cummings, 2001). Cross-correlation peak deformation can also reduce the effectiveness of subpixel peak fitting schemes which are based on a particular cross-correlation shape, such as a common five point Gaussian fit. There are both hardware and software approaches toward resolving these problems. In situations where a large in plane region must be imaged in a relatively thin device, the physics of the imaging system dictate that the entire depth of the channel will be focused. Hence a software approach must be used. Two different approaches are explored: 1. deconvolving the cross correlation with the autocorrelation and 2. image processing to replace the original particle images with unit impulse particle images.

## 2 MODELING/THEORY

### 2.1 Deconvolution Method

Simulated PIV experiments show a qualitative similarity between the cross-correlation function from a test flow containing velocity gradients in the depthwise direction and the corresponding velocity histogram for that depthwise gradient, suggesting that the deconvolution procedure may work. The major hypothesis of the deconvolution method is that the PIV cross-correlation function can be approximated by the convolution of a particle image autocorrelation with the velocity distribution in the interrogation region. This hypothesis is based on observations of cross-correlations from experimental situations. For the case of a uniform flow, the velocity distribution is an impulse, and the resulting cross-correlation can be approximated by a position-shifted autocorrelation. This suggests that the cross-correlation can be approximated by a convolution of the impulse velocity distribution and an image autocorrelation.

Olsen and Adrian (2000) approximated the cross-correlation as a convolution of mean particle intensity, a fluctuating noise component, and a displacement component. Deconvolution of a cross-correlation with an autocorrelation is used by Cummings (1999) to increase the signal-to-noise ratio for a locally uniform flow. The new idea is to extract velocity distributions by deconvolving a PIV cross-correlation function with its autocorrelation. The result is a two-dimensional approximation of the underlying velocity distribution. One drawback to deconvolution procedures is sensitivity to noise resulting from a division operation in frequency space. Thus, it is important to have high information density in both the cross-correlation and autocorrelation. The information density can be increased by correlation averaging both the cross-correlation and autocorrelation (Meinhart *et al.*, 2000).

### 2.2 Synthetic Image Method

Since deconvolution is inherently sensitive to noise, it would be beneficial to eliminate the deconvolution step from the velocity profile extraction process. This could be done if the autocorrelation were an impulse or delta function. Since the deconvolution of a function with an impulse is the original function, this would render the deconvolution operation trivial and unnecessary.

The autocorrelation is related to the particle intensity distributions from a set of PIV recordings, i.e. the shape of particles in an image pair. So, the most practical way to affect the autocorrelation is to alter the imaged shape of these particles. If the particle intensity distributions in a set of PIV recordings are reduced to single pixel impulses, the autocorrelation appears as a single pixel impulse. This desirable autocorrelation trivializes the deconvolution method such that the cross-correlation alone is equal to the deconvolution of the cross-correlation and the autocorrelation. This is the basis for the synthetic image method. Experimentally PIV recordings containing uniformly illuminated single pixel particle images can be approximately obtained by illuminating very small seed particles with a high intensity laser sheet, such that most particles are imaged by a single pixel by a digital camera. However, this approach can only be an approximation because even very small particles located near the edge of a pixel would be imaged over two neighboring pixels. Furthermore, in  $\mu$ PIV the particles are already very small, so making them any smaller could render them invisible to the camera; imaged particle intensity decreases proportionally as the cube of particle radius. Also, the image of a very small particle is dominated by diffraction optics, thus reducing the physical particle size will have very little impact on the imaged particle size due to a finite diffraction limited spot size. The typical point response function associated with microscope objectives used in  $\mu$ PIV is 5 pixels, so the desired particle intensity distribution cannot easily be obtained in raw experimental images.

### 2.3 Comparison of Techniques

Three cases were examined to compare and validate the two methods of velocity distribution extraction from cross-correlation PIV. The cases involve three different velocity profiles that are frequently encountered in  $\mu$ PIV. The first is a uniform flow (depth of field small compared to flow gradients), the second is a linear shear (near wall region of a channel flow), and the third is a parabolic channel flow (depth averaged pressure-driven flow in a shallow micro device).

#### *Uniform Flow*

The velocity profile of uniform flow is an ideal situation for making accurate PIV measurements. This case also has the simplest velocity histogram, a delta function at the uniform velocity value. The uniform one dimensional velocity profile simulated in this case study is given by  $V_x = 6.294$ . Both the deconvolution and the synthetic image methods generate the expected histograms and are shown in Figure 3. Since the histograms are calculated only at integer pixel values, they both show a peak at 6 pixels and a lower, but non-zero value at 7 pixels. By taking the average of the histogram values at 6 and 7 pixels, the true value of the uniform displacement can be found. For example in the case of the synthetic image method,  $V_{x,mean} = (6 \times 1 + 7 \times 0.46) / 1.46 = 6.32$ , which is very near the input value of 6.294.

#### *Linear Shear*

Another common flow profile is a linear shear. In microfluidics, this type of flow can be seen in the near wall region of a parabolic flow profile. Since the displacement probability density function for a linear shear has the simple shape of a top hat, this type of flow presents a good case to further benchmark the methods of deconvolution and synthetic images. This simulation case study used the velocity profile given by  $V_x = 6.294 \times Z + 1.248$  where  $Z$  is the position along the axis of the imaging system and can assume values between 0 and 1. Consequently we expect a top hat with the left edge at 1.248 and the right edge at 7.552. The results are plotted in Figure 4. The synthetic image method is a slightly better predictor of the velocity histogram than the deconvolution method by virtue of the steeper gradients at the edges of the distribution. This behavior is expected because images analyzed by deconvolution contain particle diameter and particle intensity variations, as well as slight readout noise.

#### *Parabolic or Poiseuille Flow*

The final common velocity profile to be considered is parabolic or Poiseuille flow. This type of flow is found in pressure-driven microchannel devices. Furthermore, it is the profile expected from the LOC experimental device being considered here with zero voltage applied to the DEP electrodes. This simulation used the velocity profile is given by  $V_x = 50.352 \times (Z - Z^2)$ , with  $Z$  varying between 0 and 1. Hence, we expect a velocity distribution varying between a minimum of 0 pixels at  $Z = 0$  and  $Z = 1$  and a maximum of 12.558 at  $Z = 1/2$ . The results are plotted in Figure 5. These results clearly show the increased accuracy of the synthetic image method over the deconvolution method. The synthetic image data very closely agrees with the velocity histogram. The deconvolution method suffers spurious oscillations but still gives a reasonable approximation of the velocity histogram. These spurious oscillations were initially attributed to a lack of statistical convergence, so additional image sets were added, eventually totaling ten thousand sets. The same spurious oscillations were found, so they must be inherent to this particular case. It is not typical for such oscillations to occur, but as demonstrated, the deconvolution method has definite limitations.

## 3 EXPERIMENTAL RESULTS

The experiments presented here are designed to quantify the dielectrophoretic performance of the device. The experiments used six sets of 800 images each to analyze the effect of dielectrophoresis on particle motion in the test device. These images are high quality with low readout noise, as can be seen in the example fluorescent image of Figure 6. The top image demonstrates the many different particle intensity distributions which are typically present in a  $\mu$ PIV image in which the particles are distributed randomly within the focal plane. The bottom figure shows how, as the result of the DEP force, the particles migrate to the top of the channel and all have nearly identical images. The top image also shows that when a significant DEP force exists, the particles are trapped at the electrode locations by the increase in DEP force there. In general, the observed particle image shape is the convolution of the geometric particle image with the point response function of the imaging system. The point response function of a microscope is an Airy function when the point being imaged is located at the focal plane. When the point is displaced from the focal plane, the Airy function becomes a Lommel function (Born and Wolf, 1997). For a standard microscope the diffraction limited spot size is given by

$$d_e = \frac{1.22 \cdot \lambda}{NA} \quad (1)$$

A numerical aperture (or NA) of 1.00 and an incident light wavelength  $\lambda$  of 540nm results in a diffraction limited spot size of 0.66 $\mu$ m, while the particles used are 0.69 $\mu$ m. Consequently the particle intensity distributions as recorded by the camera are partly due to the geometric image of the particle and partly due to diffraction effects. Hence, the distance of any particle from the focal plane can be determined by the size and shape of the diffraction rings.

Two different PIV analyses were performed. Initially a conventional  $\mu$ PIV analysis was performed to obtain an estimate of the average particle velocity field. Because the goal of the conventional  $\mu$ PIV analysis is not to extract velocity distribution, only the median velocity is reported. Figure 6 shows vector plots for the experimental cases of 0.5 volts (top) and 4.0 volts (bottom). A uniform color scale was applied to these figures for representing velocity magnitude, such that velocity changes between cases can be more easily interpreted.

A second type of PIV analysis was performed in which the velocity distribution within each interrogation was extracted by either deconvolving the autocorrelation function for the interrogation spot with the cross-correlation function or by using an image processing technique. This approach reveals more about the particle dynamics because there are considerable gradients in the depthwise direction in this case. The two cases used in Figure 6 are replotted again in Figure 7 as probability density functions. The increase in the richness of the information is clearly evident although its interpretation is far from straightforward.

A preliminary investigation of the results reveals some very interesting particle dynamics in this device. For example, initially the average particle velocity increases as the voltage increases. This phenomenon is explained by particles being displaced from the channel bottom into faster areas of the fluid flow. This biases the velocity distribution toward higher velocities, altering the shape of the cross-correlation peak to favor higher velocities even though the fluid flow is constant. For higher voltages the effect of particles being hindered by axial field gradients is compounded by particles being forced beyond the high speed central portion of the flow profile by the DEP force. It can be qualitatively confirmed that particles migrate to the top of the channel by observing particle shapes in the images from the higher voltage cases, i.e. comparing the many particle shapes found in Figure 2 (top) which is acquired at 0.5 volts with the single particle shape found in Figure 2 (bottom) which is acquired at 4.0 volts. It is confirmed that the particles are indeed at the top of the channel by traversing the focal plane throughout the depth of the device. Furthermore, the rapid fluctuations in the particle velocities inside the device call into question whether the steady drag assumption, which is used in nearly all DEP particle dynamics equations, is appropriate.

#### 4 CONCLUSIONS

The dynamics of particles traveling through the device described in this paper are very complicated, exhibiting migration normal to the electrodes as well as trapping behavior in the plane of the electrode. Several novel PIV interrogation techniques are applied to shed light on the particle dynamics. Further work is needed to assess the accuracy of the steady drag assumption.

#### REFERENCES

- M. Born, E. Wolf, Principles of optics, Oxford Press, Pergamon, 1997.
- E.B. Cummings, "An image processing and optimal nonlinear filtering technique for PIV of microflows", Experiments in Fluids, Vol. 29, [Suppl.]:S42-50, 2001.
- HB Li, Y Zheng, D Akin, R Bashir, "Characterization and Modeling of a Micro-Fluidic Dielectrophoresis Filter for Biological Species," submitted to J. Microelectromechanical Sys. (2004).
- C.D. Meinhart, S.T. Wereley, J.G. Santiago, 2000, "A PIV algorithm for estimating time-averaged velocity fields," J. Fluids Eng., Vol. 122, 809-814.
- M.G. Olsen, R.J. Adrian, 2000, "Out-of-focus effects on particle image visibility and correlation in microscopic particle image velocimetry," Experiments in Fluids, [suppl.], S166-S174.
- S.T. Wereley, L. Gui, C.D. Meinhart, "Advanced Algorithms for Microscale Velocimetry," AIAA J., Vol. 40, No. 6, 1047-1055, 2002.

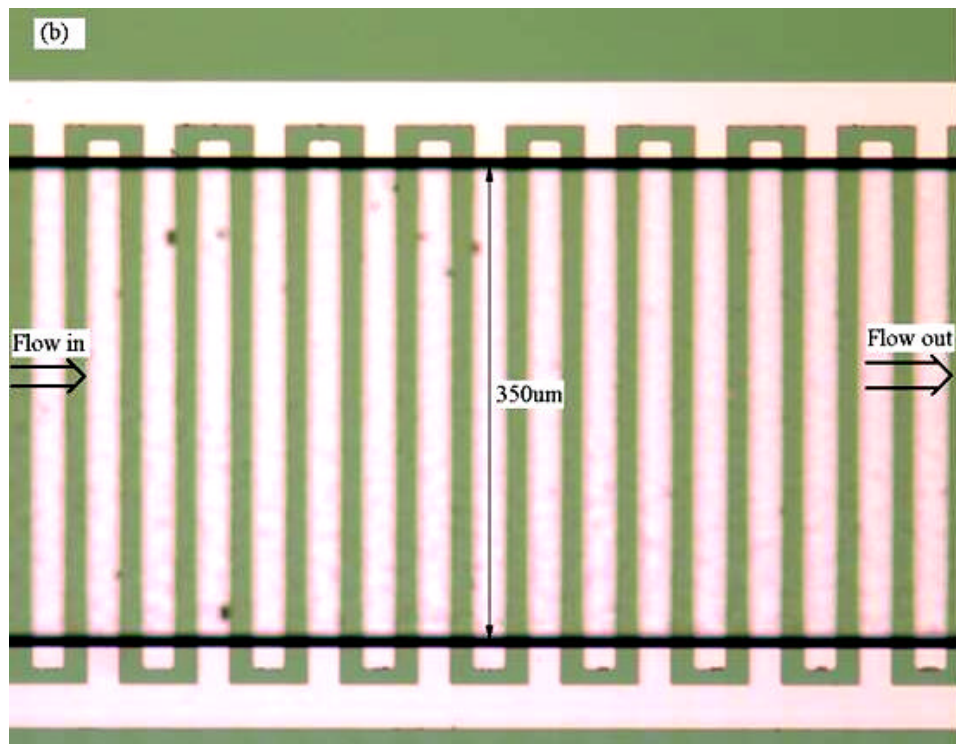
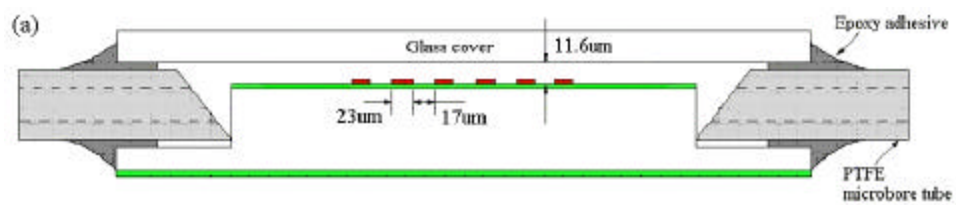


**Figure 1.** (a) Schematic view of experimental apparatus and (b) photo of apparatus.

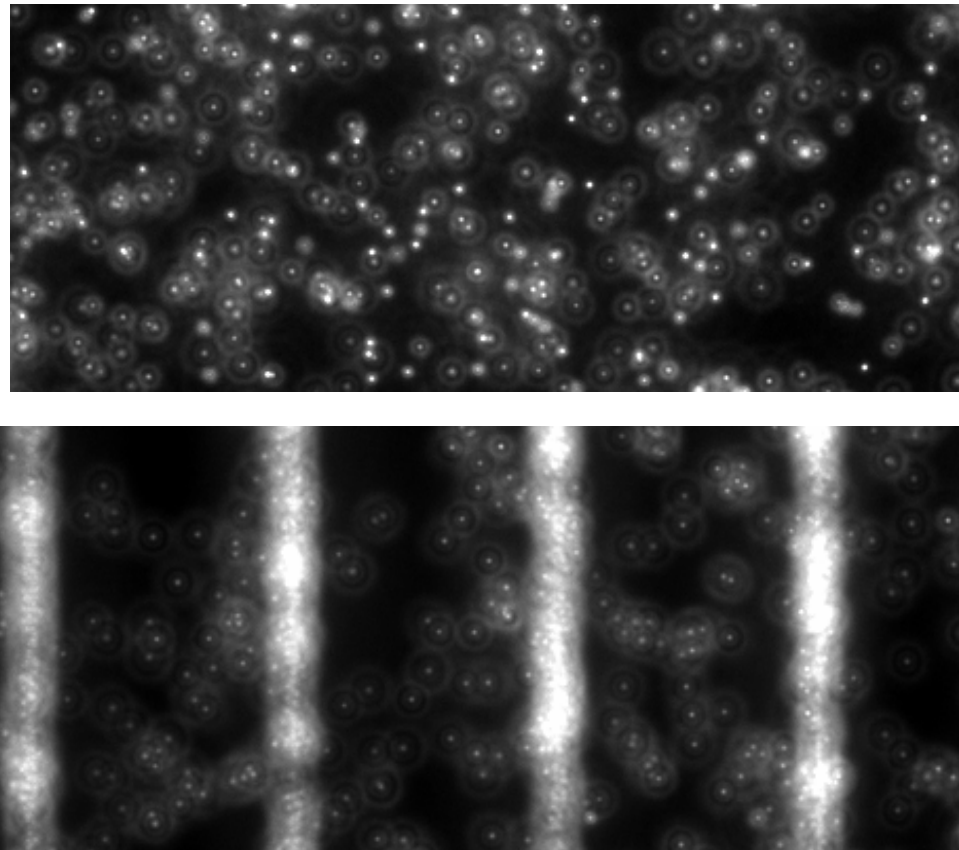


**Figure 2.** A photo of PSL particles with 0.0 volts (top) and 4.0 volts (bottom).

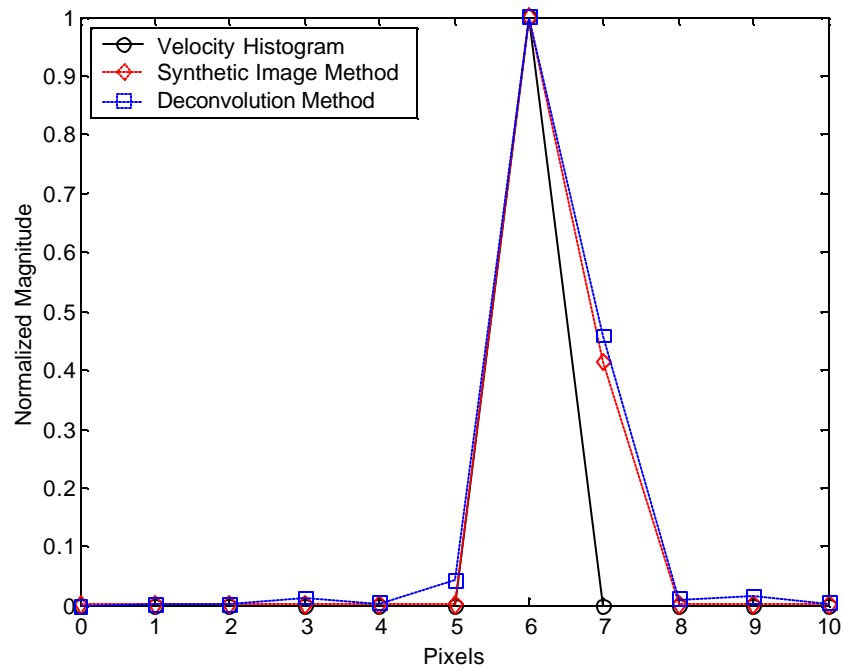


**Figure 3.** Uniform flow simulation results,  $V_x = 6.294$ .

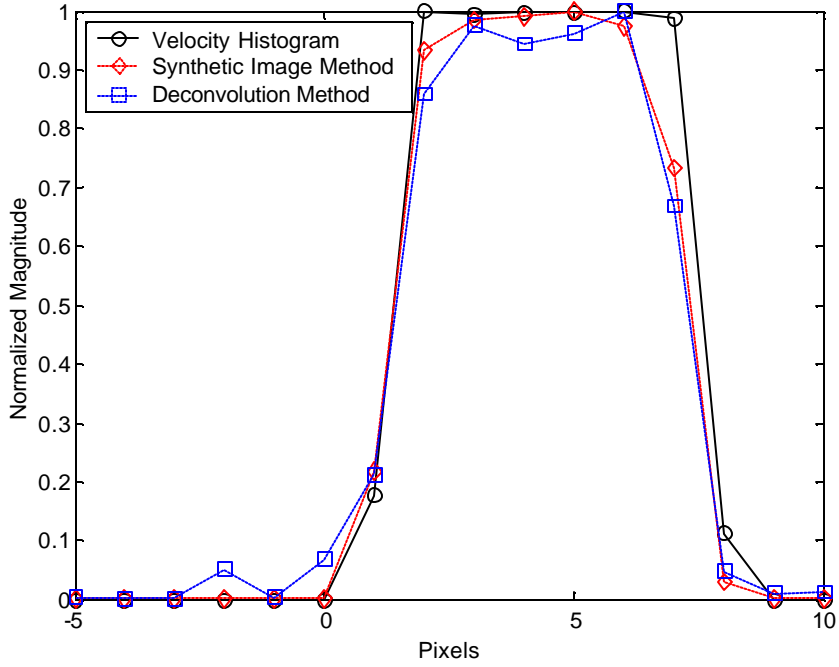


**Figure 4.** Linear shear simulation results,  $V_x = 6.294 \cdot Z + 1.248$ .

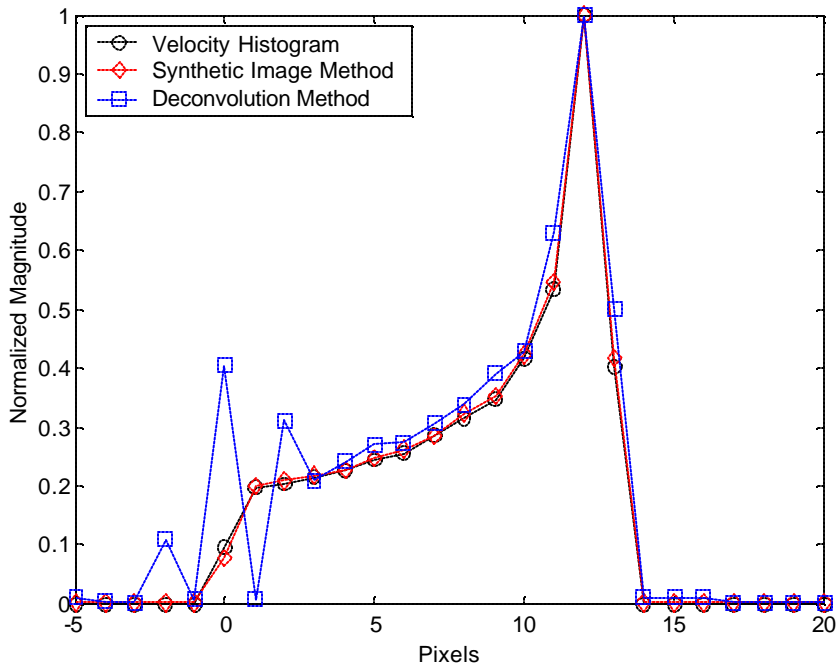


**Figure 5.** Parabolic flow simulation results,  $V_x = 50.352 \cdot (Z - Z^2)$ .

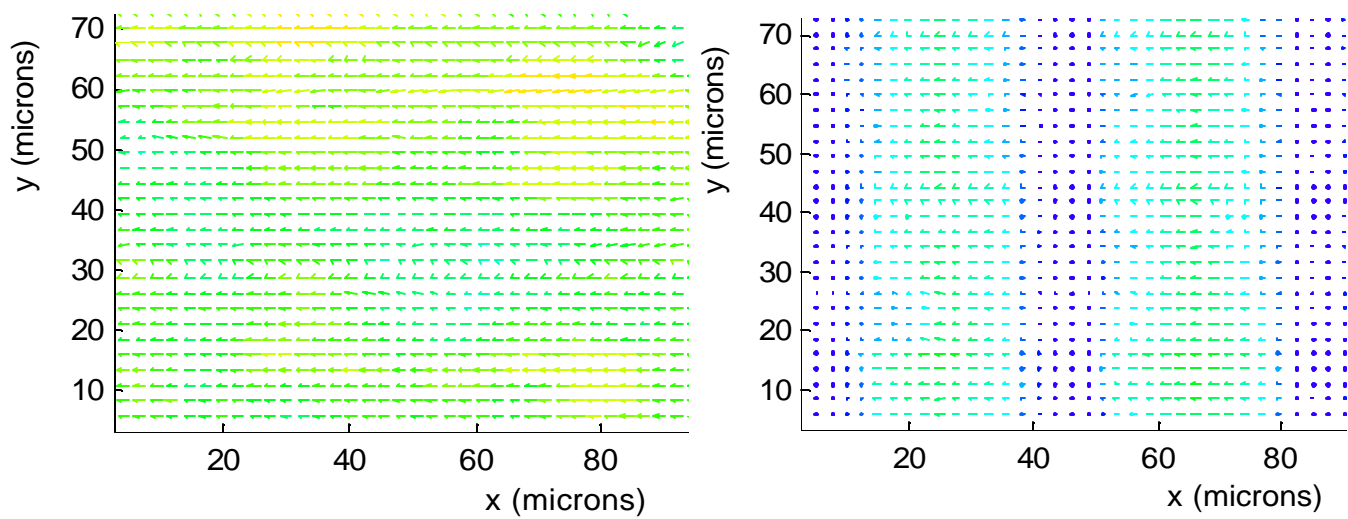


**Figure 6.** PIV vector plots for electrode voltages of 0.5 volts (top) and 4.0 volts (bottom).

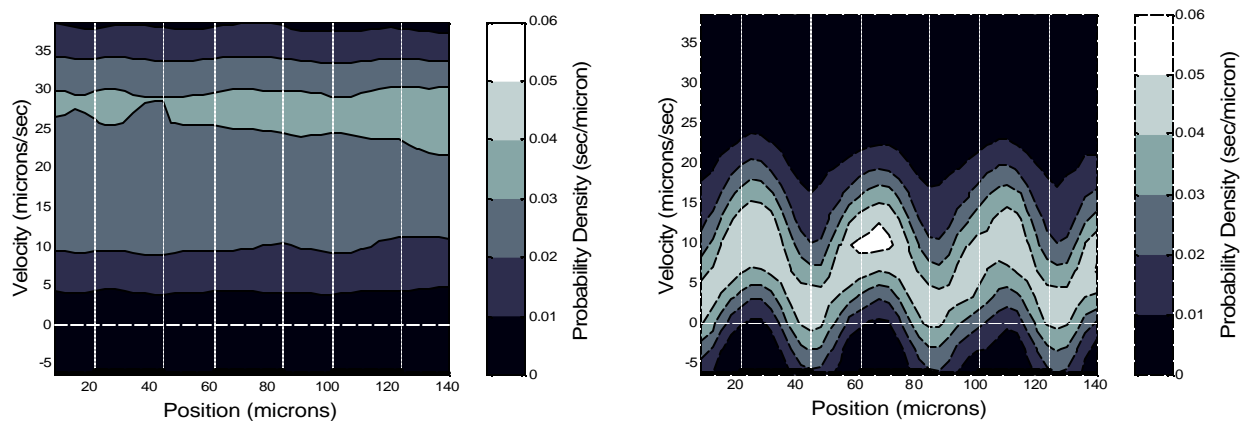


**Figure 7.** Probability density function for axial particle speed as a function of axial position within the DEP particle trap.